J. Appl. Comput. Mech., 5(2) (2019) 258-268
DOI: 10.22055/JACM.2018.26297.1318

ISSN: 2383-4536
jacm.scu.ac.ir

M&MoCS

Shahid Chamran University of Ahvaz

Journal of Applied and Computational Mechanics

Research Paper

Accuracy Assessment of Ultrasonic C-scan and X-ray Radiography Methods for Impact Damage Detection in Glass Fiber Reinforced Polyester Composites

Seyyed Abbas Arhamnamazi[1], Nasrollah Bani Mostafa Arab[1], Amir Refahi Oskouei[1] Francesco Aymerich[2]

[1] Mechanical Engineering Department, Shahid Rajaee Teacher Training University, Tehran, Iran

[2] Mechanical, Chemistry and Material Engineering Department, University of Cagliari, Cagliari, Italy

Received June 19 2018; Revised August 19 2018; Accepted for publication September 07 2018.
Corresponding author: N. Bani Mostafa Arab, n.arab@sru.ac.ir

Abstract. The present study introduces two quantitative parameters to compare the accuracy of ultrasonic C-scan testing and X-ray radiography methods in the damaged area detection under low-velocity impact in polymer-based composites. For this purpose, the hand lay-up technique of composite processing was employed to prepare the composite specimen. A composite specimen consisting of the glass fiber reinforced with the unsaturated polyester resin was considered for this investigation. The impact tests at different energy levels were carried out to create three damaged areas in this composite specimen. Because the glass/polyester specimen had a transparent surface, a digital scanner was used to obtain an ideal image of specimen representing the region and edge of the impacted areas. Two image quality factors were introduced as quantitative parameters to compare the ultrasonic C-scan and X-ray radiography results with those of an ideal image. The results of this study showed that the ultrasonic C-scan is a more accurate method for inspection of the GFRP specimen.

Keywords: Composites; Damage zone; Ultrasonic C-scan; X-ray Radiography.

1. Introduction

Composite materials have a wide range of applications in various industries such as aviation, space, boat, building, and automotive [1]. Polymer-based composites, especially the fiberglass reinforced plastic (GFRP), are used widely for their special properties like low fatigue, good thermal and acoustic insulation, high stiffness to weight and strength to weight ratios, and better mechanical properties in comparison to metals [2]. Despite these properties, when they are subjected to various types of loading under service conditions, the defects may initiate and develop in these materials, which can lead to their failure. The defects are defined as any deviation from the ideal structure or component. The impact damage is a common defect that may occur during manufacturing or in-service application of composites [3]. Because impacts are the primary cause of delamination, it is necessary to assess composites production using non-destructive testing (NDT) methods, which enable the detection of damaged areas.

Several studies have been conducted on the impact damage detection using various NDT methods. To name a few, Maierhofer et al. [4], Usamentiaga et al. [5], and Meola and Carlomagno [6] used the thermography-based method to find the impact damage area in CFRP and GFRP specimens. They found that thermography can find the defects, but deep defects and delamination cannot be detected completely. Although Usamentiaga et al. claimed that their method is able to detect all defects correctly, but their results did not represent such a high quality. Liang et al. [7], Cheng et al. [8], and Koyama et al. [9] used Eddy Current Testing (ET) method. Liang et al. reported that the eddy current pulse thermography shows a better ability to

Published online: January 20 2019

detect small defects in the CFRP sample in comparison with the thermography technique. Rauter and Lammering [10] and Capriotti et al. [11] used the guided wave to detect the damage. Rauter and Lammering reported their method can find the micro-structural damage in CFRP materials. Hasiotis et al. [12] and Shen et al. [13] used ultrasonic C-scan for impact damage detection in CFRP materials; they could detect all defects in their experiments. Ono et al. [14], Amoroso et al. [15], and Chandarana et al. [16] used Acoustic Emission (AE) to monitor the materials during the manufacturing process as well as the service time to find the defect area in CFRP specimens. Some studies used emerging NDT methods for impact damage detection in composite materials. For example, Yunze et al. [17] used volume heating thermography (VHT) and inside heating thermography (IHT) for advanced composite materials. Yunze et al. [18] used nonlinear ultrasound (NU) and vibro-thermography (VT) NDT based on the shared excitation sources to detect barely visible impact damage areas in CFRP samples. He et al. [2] reported that the pulse eddy current shows a higher reliability and a better defect detectability for deep defect in honeycomb composite materials in comparison with optical methods like flash thermography and shearography. Other studies used two or more methods to compare their ability and accuracy in the damaged area detection. For example, Cantwell et al. [19] and Ravikiran et al. [20] used ultrasonic C-scan and Radiography, Chambers et al. [21] used acoustic emission and X-ray radiography, Pieczonka et al. [22] used vibrothermography, shearography, and Ultrasonic C-scan to identify the place of impact damaged area. Measuring the defect area is important because the larger the defect size in a structure, the less its service life is. Therefore, it is necessary to find a quantitative parameter to evaluate and compare the accuracy of various NDT methods for defect detection.

In this study, the GFRP plate was produced and subjected to the impact test. Because of the transparency of this specimen, it can be scanned digitally to have an ideal image that demonstrates a clearly visible damaged area. Accordingly, the ultrasound C-scan and X-ray radiography methods were used to find and measure the size of the impact defects. Moreover, two quantitative Image Quality Assessment (IQA) parameters were introduced to compare the accuracy of NDT methods in order to detect the impact area. The IQA values of C-scan and radiography images were calculated with respect to the digital scan image (as an ideal image) in order to verify the precision of these methods in defect detection process of GFRP specimen.

2. Materials and Methods

2.1. Test Specimen Preparation

Two E-glass woven rovings with the area densities of 200 and 400 g/m^2 were used as reinforcements. The former was supplied by Camelyaf Company, Turkey, and the latter was from Saze Morakab Company, Iran. A matrix composed of the unsaturated polyester resin BUSHPOL 751129 with 40 wt. % styrene as a solvent with a viscosity of 6500 cP was supplied from Bushehr Chemical Industry, Iran. Moreover, Methyl Ethyl Ketone Peroxide (MEKP) was used as initiator and Cobalt Naphthenate was used as the accelerator; they were purchased from Iran Peroxide Company and AKZO Nobel, respectively. The composite plate was made of the glass fiber along with the polyester resin using the hand lay-up method under the vacuum condition. The test specimen with dimensions of 222mm × 150mm × 3mm with 6 layers was produced.

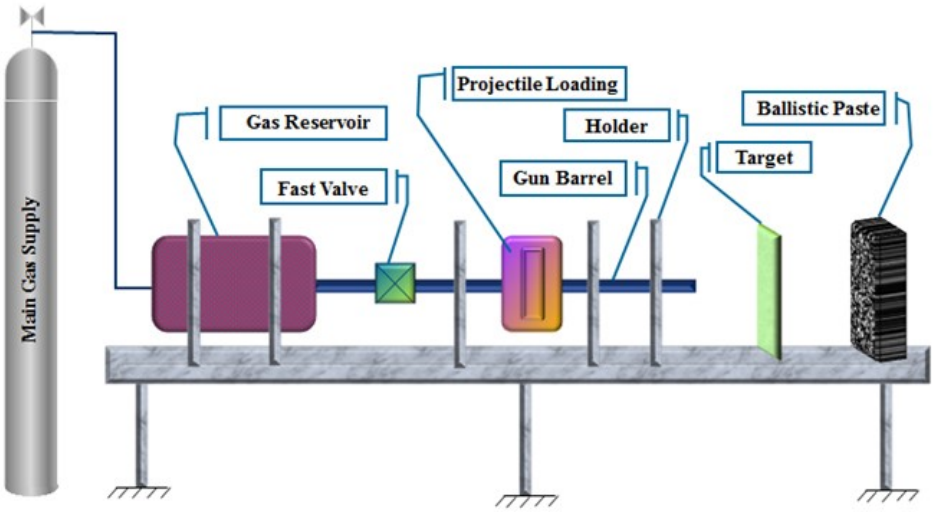

Fig. 1. Impact testing device.

2.2. Impact Test

Impact tests were conducted by employing a gas-gun instrument (Fig.1). The gas-gun had a long smooth barrel (3 m) with an interior diameter of 8.7 mm, a pressure release valve that could act fast, a unit for loading projectile, a supply gas vessel, a gas reservoir with the volume of 500 ml for each shot, a target holder, and a ballistic paste to cease the projectile without any disruption. For all impact tests, a hardened steel spherical projectile with a diameter of 8.7 mm was utilized. Because of the gas pressure, the projectile was propelled from the gun barrel and collided with the specimen. If the projectile had a high velocity, it could have passed through the specimen and stopped in the ballistic paste. In order to test the accuracy of NDT methods, it was important to have impact-damaged areas in the specimen that were not visible to the naked eye. According to Nasirzadeh

and Sabet [23], there is a linear relation between various gas pressures and initial projectile velocities (also initial projectile energy) at low pressures. Therefore, the gas pressure can be changed such that the projectile does not pass through the specimen to have invisible impact damage areas. Impact test was repeated three times to ensure the repeatability of the results.

2.3. Ultrasonic C-scan Method

The Ultrasonic pulse-echo immersion C-scan was used to assess the specimen subjected to the impact. The specimen was tested using a focused broadband transducer (14 mm diameter, 27 mm focal length) with a center frequency of 1 MHz. The ultrasonic testing system had a scanning bridge with a resolution of 0.025 mm, a 150 MHz Krautkramer HIS2 ultrasonic pulser/receiver, and a 500 MHz Hewlett Packard 54520A digital oscilloscope used for the acquisition of the ultrasonic signals. A personal computer was used to control the scanning process and trigger the pulser/receiver of emission and acquisition of ultrasonic pulses. At each point of the scanning process, the ultrasonic waveforms were digitized and stored in the internal buffer of the oscilloscope. Finally, the digitized signals were transferred to the computer. Fig. 2 illustrates a schematic sketch of the experimental setup of immersion pulse-echo testing of the specimen. The ASTM E494-10 standard was used for the ultrasonic test procedure. According to this standard, the specimen surfaces that are in front of the probe should be perpendicular to the direction of flow energy and must have a surface finish of at least 3.2μm and be at most ± 3° non-parallel. To scan the surface of the specimen, the scanning steps along the length and width of it were considered to be 1 or 0.2 mm.

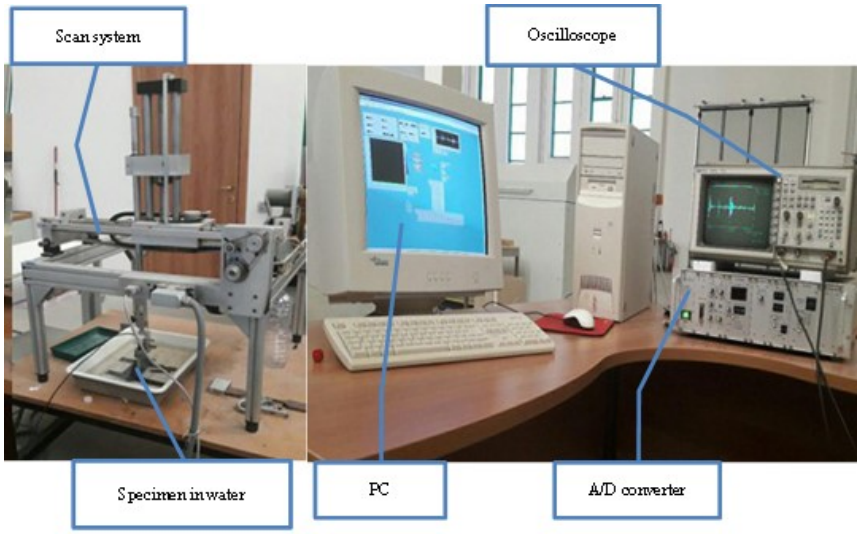

Fig. 2. Schematic diagram of the ultrasonic C-scan test.

2.4. Radiography Testing Method

A nondestructive penetrant-enhanced X-ray analysis was used for composite specimens to assess the extent of the impact-induced damage. At first, the specimens were immersed in a radio-opaque zinc iodide solution (60 g zinc iodide, 10 ml water, 10 ml isopropyl alcohol, and 6 ml Kodak Photoflo [24]) for 5 h. Therefore, the solution permeated in damaged areas and enhanced the contrast between the damaged and intact regions by changing the X-ray absorption coefficient in damaged areas. Then, the specimens were cleaned carefully with acetone and radiographs were made using an HP Faxitron cabinet (model 43855A). The radiographic system consisted of a self-rectified X-ray generator with a tube current of 3 mA and a voltage output continuously adjustable between 10 and 130 KV. The X-ray equipment had an X-ray source and Beryllium window with the size and thickness of 0.5 and 0.64 mm, respectively. Therefore, it could provide radiographic images with high resolution for small to medium size specimens. In order to set the exposure settings and providing the best image quality, radiographic exposures were preliminarily made using voltages varying from 20 to 50 kV and irradiation times ranging from 60 to 300 sec. for the GFRP specimen. The final radiographic images were obtained using a 30 kV voltage, a 3 mA current, and a 180 sec exposure time to produce X-ray images on a fine grain AGFA NDT D4 film placed immediately below the under-investigation specimen plate. The film and the X-ray source had an approximate distance of 60 cm. After film processing, digital images of the film were prepared using a digital scanner (Canon DR-F120) at a resolution of 600 dpi for the direct observation of damage and the measurement of the projected delaminated areas.

2.5. Image Quality Assessment

The image quality assessment is a very important issue in the image processing. The image quality is defined as the visibility of distortion in the color, shifts, blurriness, and Gaussian noise of a given image that can be done subjectively or objectively [25]. In a subjective way, human observers evaluate the quality of images. This method is the most accurate and reliable one but it is expensive and time-consuming. The objective IQA methods consider mathematical models that can anticipate the quality of an image precisely and automatically. An ideal objective IQA method should be able to emulate the quality predictions of an average human observer [26-27]. Mean Square Error (MSE) is a prevalent objective IQA, which is defined as the power of the difference between the reference and test images. MSE value can be calculated using the following

equation:

$$MSE=\frac{1}{WH}\sum_{j=1}^{H}\sum_{i=1}^{W}\left[I_{ref}(i,j)-I_{test}(i,j)\right]^2 \quad (1)$$

where W and H represent the width and height of the images, and I_{ref} and I_{test} denote the reference and test images, respectively. The peak signal to noise ratio (PSNR) commonly is utilized as an objective IQA. This parameter is calculated by considering the MSE value. PSNR is the maximum possible power of a signal to power distortion ratio, which is calculated by:

$$PSNR=10\times\log\left(\frac{D^2}{MSE}\right) \quad (2)$$

where D denotes the dynamic range of pixel intensities; e.g., for an 8 bits /pixel image D is 255 [28]. Besides, the PSNR is measured in decibels (dB). Higher values of PSNR and MSE indicate higher and less similarity between test and ideal images, respectively [29]. In this study, the binary images of the outputs of ultrasonic and radiography methods were considered as test images while the output of the digital scanner was the ideal image.

2.6. NDT data fusion results

The NDT data fusion can be obtained by combining NDT images and using a signal-processing concept. The NDT data fusion helps to increase the knowledge about the defect location and characterization and reduce obscurity. The aim of this process is to evaluate the structural integrity of a material more accurately [30-31]. Several NDT data fusion processes are applied to perform fusion of ultrasonic C-scan and radiography images at the pixel level. The maximum amplitude is obtained by comparing pixel values and selecting the maximum amplitude of images. The integration is acquired by using "and" operation of pixel values. The Bayesian analysis can be obtained by Eq. 3,

$$p(d_i/p\nu)=\frac{p(p\nu/d)p(d_i)}{\sum_i p(d_i)p(p\nu/d_i)} \quad (3)$$

where p(d) is the prior probability of having a defect (d) in the specimen, and $p(d/p\nu)$ is the posterior probability of hypothesis (d) using the pixel value. The probability of defect occurrence usually assumes as 50% ($p(d)=50$) [30]. Such probabilities for the ultrasonic C-scan and the radiography images are denoted as $p(p\nu/d)_U$ and $p(p\nu/d)_R$, respectively.

3. Results and discussion

3.1. Ultrasonic Results

3.1.1. Ultrasonic A-scan

An immersion focal ultrasonic probe was used in this study because it can highly focus on the ultrasonic sound pressure at a special point and detect very small discontinuities. In addition, it ignores non-relevant indications outside the focal length. Fig. 3 illustrates the setup of ultrasonic pulse-echo immersion testing. A-scan signal corresponding to Fig. 3 setup is shown in Fig. 4. In these figures, D_1 is the distance between the probe and the specimen, D_2 is the distance between the specimen and the bottom of water reservoir (height of support), T is the thickness of the specimen, FS is the front surface echo, BW is the back wall echo of the specimen, and R is the echo from the bottom of water reservoir. Figs. 4(a) and 4(b) demonstrate the signals for intact and impact areas, respectively. By comparing these signals, it can be observed that the BW and R echoes disappear or shift in the impact areas.

In addition, $2t_1$ is the pulse-echo time delay between the front surface of the specimen and the probe, $2t_2$ is the pulse-echo time delay between the front surface and the back wall of the specimen, and $2t_3$ is the pulse-echo time delay between the back wall of specimen and the bottom of water reservoir (Fig. 4(a)). These parameters suggest the following relations:

$$2t_1=\frac{D_1}{V_W} \quad (3)$$

$$2t_2=\frac{T}{V_{sp}} \quad (4)$$

$$2t_3=\frac{D_2}{V_W} \quad (5)$$

where V_W is the sound velocity in water and V_{sp} is the sound velocity in the specimen.

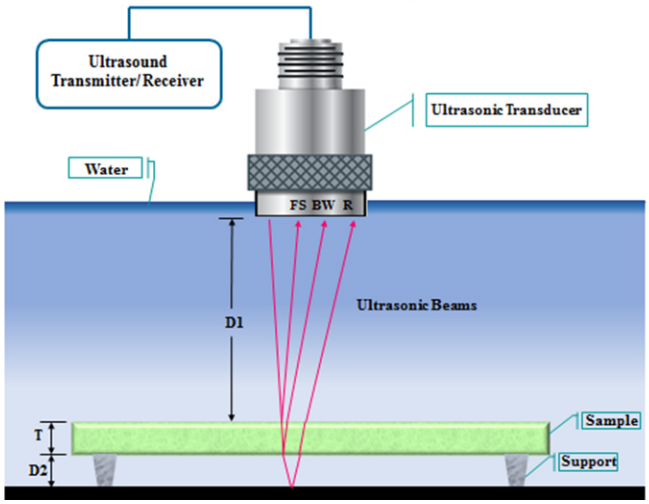

Fig. 3. Schematic diagram of ultrasonic Immersion pulse-echo.

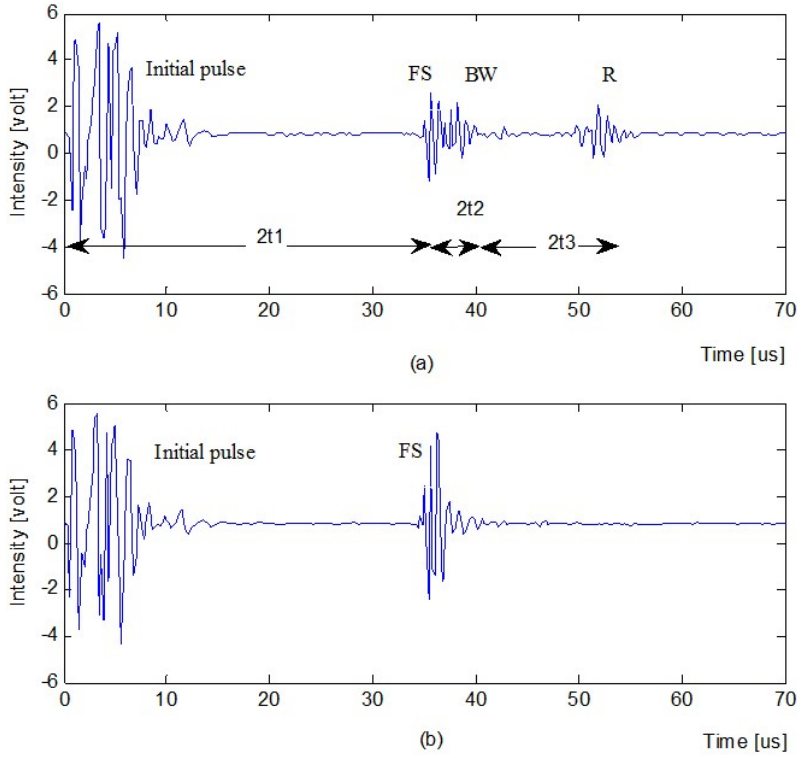

Fig. 4. The signal acquired from the setup shown in Fig. for: (a) intact areas (b) impacted areas.

3.1.2. Ultrasonic C-scan Results

If the surface of the specimen is parallel to the ground surface, the FS echo does not shift with changing the location of the probe on the top of the specimen. In the C-scan test, there are two types of signals (as shown in Fig. 4(a) & (b)). If the probe is on the top of the damaged area, BW echo is attenuated because of scattering in the entrance signal. In contrast, if the probe is on the top of the undamaged area, the BW echo is not attenuated. After adjusting A-scan, all the surface of the specimen should rapidly be checked to understand that the specimen surface is parallel to the probe scan surface. In the present study, a focal probe was used for the ultrasonic C-scan method. In this probe type, it is possible to adjust the probe-specimen distance to have a maximum energy of signals at a particular point and reduce the scattering noises. The maximum amplitude of back wall echo was considered as a parameter to distinguish the impact and intact areas. Therefore, the focal point was set on the back surface of the specimen. For this purpose, a D_1 parameter as in Fig. 3 was adjusted according to Eq. 3 to obtain the maximum amplitude of back wall echo. Finally, the probe (Fig. 5) scanned the top surface of the specimen. To save time, the first step is that all the surface has to be scanned with the step size of 1 mm at X and Y directions. The C-scan results of this step using the maximum amplitude of back wall (BW echo is demonstrated in Fig 4(a)) for the specimen is shown in Fig. 6(a). After identifying the location of the defect, these locations were retested with a step size of 0.2 mm at X and Y directions to determine damaged areas more accurately. These results are shown in Figs. 6. three damage areas in the specimen were detected. In addition, there are some defect-free areas wherein the back wall echo was attenuated. This result can be attributed

to the high scattering of woven fibers, wrinkle defects, and irregularity of woven fibers distribution in the specimen. This result can be attributed to the high scattering of woven fibers, wrinkling, and irregularities of fiber distribution in the specimen.

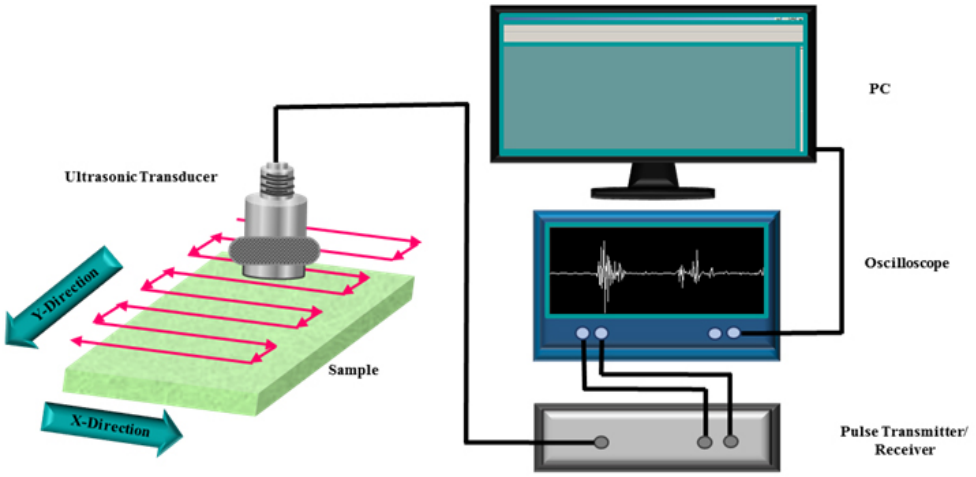

Fig. 5. Schematic diagram of the ultrasonic C-scan

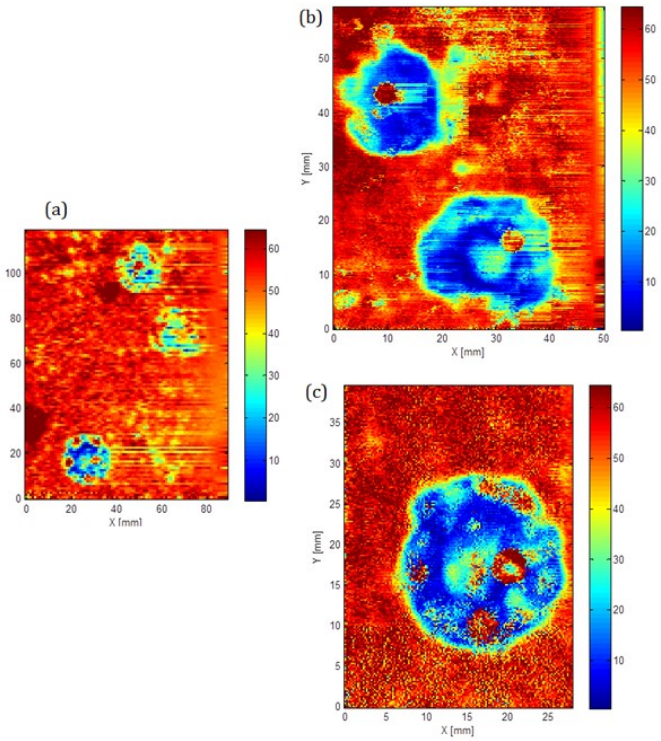

Fig. 6. The result of ultrasonic C-scan for the specimen: (a) scan of all specimen surface with the step of 1mm, (b), and (c) scans of damaged areas with the step of 0.2 mm.

3.2. Radiography Results

For the specimen, the fiberglass woven distribution was not uniform in all parts of the specimen. Moreover, X-ray absorption coefficients between damaged and intact regions were not significantly different while the scattering level was very high. Accordingly, it was very hard to achieve a high-quality X-ray image of the specimen. To obtain a best-quality X-ray image for evaluating the specimen, a test setup was designed at six different levels based on voltage and exposure time factors (Table 1). Fig. 7 illustrates the results of X-ray radiography of the specimens by changing radiography parameters based on Table 1. As can be noted, the image of second setup (with a voltage of 40 kV and an exposure time of 180 sec) is completely dark and thus is not reported in Fig. 7. According to Fig. 7, the best was achieved with a voltage of 30 kV and an exposure time of 180 sec. Besides, it was found that the X-ray radiography is not a good method to detect the defect in the GFPR specimen because at some particular voltages and exposure times, the edge of defects cannot be identified clearly due to the high X-ray absorption coefficient of glass fibers.

Table 1. Various setup conditions for the X-ray radiography testing of the specimen.

Number of setup	Voltage (kV)	Exposure time (s)
1	50	60
2	40	180
3	30	300
4	30	180
5	20	150
6	20	90

3.3. Image Quality assessment

To compare the accuracy of NDT methods, it is necessary to know the real size of the defect. In previous studies, artificial defects were created using a thin layer of Teflon with a specified size between layers of composite [12] or drilling a bottom flat hole on one side and testing the specimen from another side [32]. Destruction of the specimen is another solution to achieve the real size of artificial defect [33]. In the first solution, all layers above the artificial defects exhibit a small bending over the defects [12]. Therefore, the real size of the defect is larger than the embedded Teflon layer (the size of the artificial defect). In the second solution, the peel-up or delamination may occur during the drilling process. Therefore, in this case, the size of the artificial defect is larger than the drill bit diameter. In the destructive method, the real size of the defect can change. Taking these together, it is necessary to have another method for measuring the real size of artificial defects.

In this study, the GFRP specimen was selected for its transparent property. The size of the impact area can be detected accurately using a digital scanner (Canon DR-F120). Fig. 8(a) shows the ideal image, which is acquired from the digital scan of the impacted GFRP specimen. Fig. 8(b) is obtained from Fig. 8(a) using an adaptive Niblack's Algorithm [32] to convert it into a binary image. In this image, the impact areas are white and the intact regions are black. Fig. 9(a) illustrates the C-scan result of GFRP specimen by inserting Figs. 6(b) and 6(c) into the exact place of impact damage areas to improve Fig. 6(a). In Fig. 9(b), an adaptive Niblack's Algorithm [34] is used to convert Fig. 9(a) into a binary image and distinguish impact (white regions) and intact (black regions) areas. Fig. 8(b) is resized by considering the relation between the number of pixels and the real size of the specimen, which was measured by a caliper. Fig. 9(b) is resized by considering the scan step of C-scan that was 0.2 mm in X and Y directions. Fig. 10 presents the binary of X-ray radiography image of the specimen. This image is resized by considering the size of radiography film. It is clear that Fig. 9(b) is highly similar to Fig. 8(b), proving the high accuracy of the ultrasonic C-scan method for damage detection in the GFPR specimen. In contrast, Fig. 10 is not similar to Fig. 8(b) and the edges of defect areas are not clear. Therefore, the X-ray radiography is not an accurate method for damage detection in the GFPR specimen.

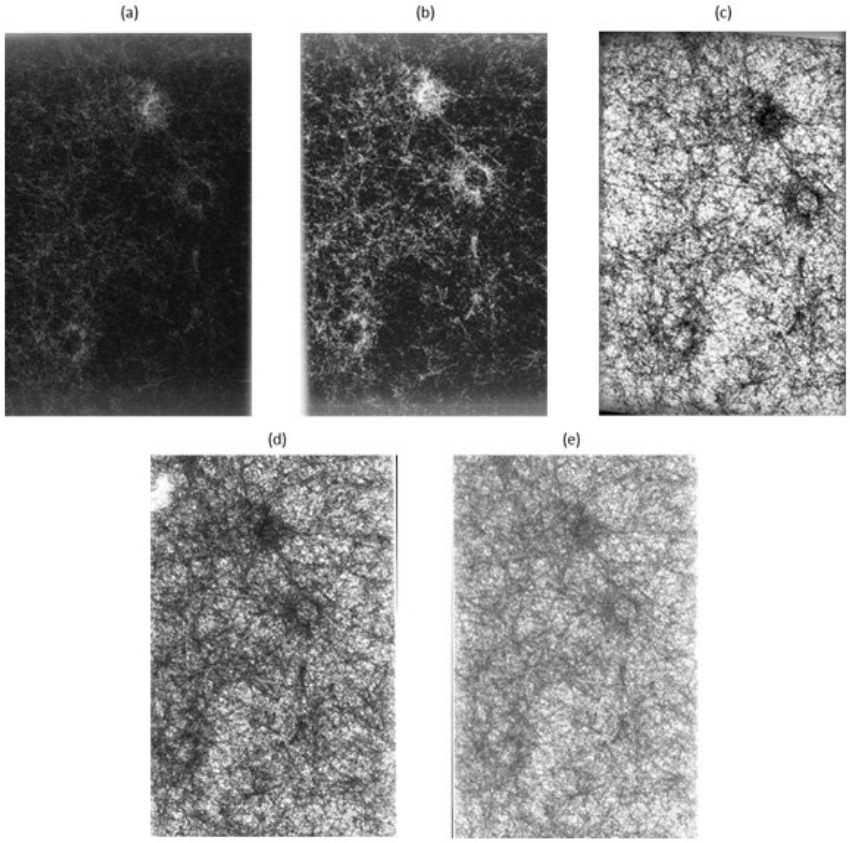

Fig. 7. Digital scan of X-ray images obtained from the specimen in: (a) a 50 kV voltage and exposure time of 60 sec (b), a 30kV voltage and exposure time of 300 sec, (c) a 30kV voltage and exposure time of 180 sec, (d) a 20kV voltage and exposure time of 150 sec, and (e) a 20kV voltage and exposure time of 90 sec.

Moreover, these images have the same pixel/mm size and are comparable to calculate MSE and PSNR as in Eqs. (1) and

(2). The values of MSE and PSNR, according to these equations, are given in Table 2. Based on these equations, it can be proved that a decrease in the MSE and an increase in the PSNR lead to a consequent increase in the accuracy of the test image (the results of NDT methods). Therefore, the accuracy of the C-scan method is more than that of the X-ray radiography method for the GFRP specimen. Moreover, the impact areas can be measured using the ideal image, C-scan, and X-ray radiography. For this purpose, images were calibrated by considering the dpi of scan images (for radiography and ideal images) or the scan step (for ultrasonic C-scan results) in the ImageJ software. Measured impact areas for higher, middle, and lower damaged areas in the CFRP sample are given in Table 3 (According to Fig. 8 (a)). The error obtained from the C-scan method (5.09%) is considerably less than that of the X-ray radiography method (39.04%).

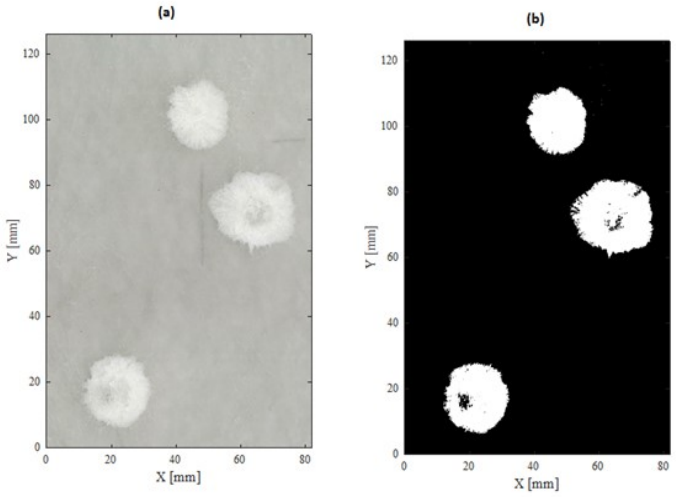

Fig. 8. (a) Digital scan of the specimen and (b) binary image of (a).

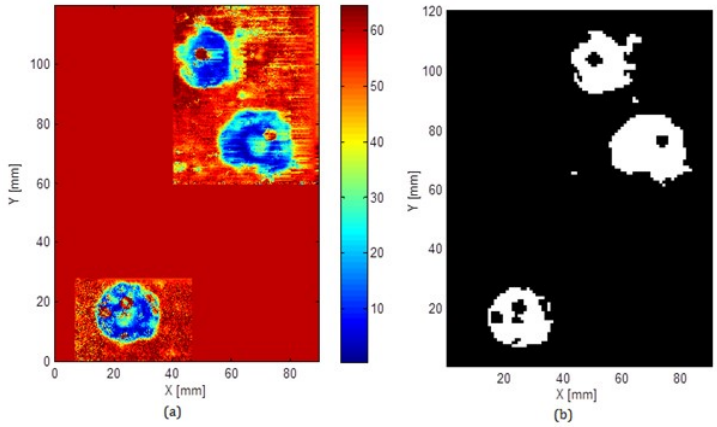

Fig. 9. (a) Ultrasonic C-scan of the specimen by selecting Fig. 6 (b) and (c) in the exact place of impacted damage areas to obtain the complete scan of the specimen and (b) the binary image of Fig. 9 (a).

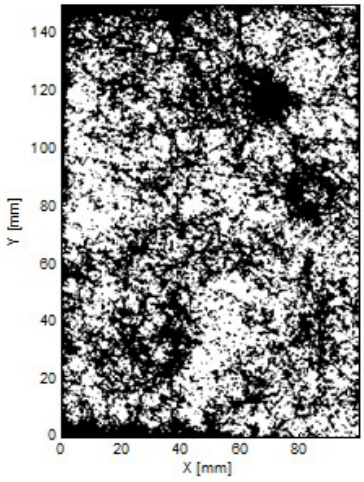

Fig. 10. The binary image of the X-ray radiography

Table 2. The MSE and PSNR values for the ultrasonic C-scan and X-ray radiography methods.

Methods	MSE	PSNR
C-scan	0.0017	174.4951
X-ray radiography	0.0050	163.8222

Table 3. Impact region areas calculated using the ultrasonic C-scan and X-ray radiography methods.

Defects	Digital Scan	C-scan		X-ray Radiography	
	Area (mm^2)	Area (mm^2)	Error (%)	Area (mm^2)	Error (%)
Higher damage area	328.448	314.92	4.12	158.495	51.74
Middle damage area	486.432	453.96	6.67	324.130	33.37
Lower damage area	364.666	350.60	3.86	236.380	35.18
Total	1179.546	1119.48	5.09	719.005	39.04

3.4. NDT data fusion results

By using data fusion techniques, more reliable results can be acquired [31]. Figs. 11(a) and (b) were obtained from integration and maximum amplitude NDT data fusion methods, respectively. The results of the Bayesian approach were achieved by combining the data from NDT images by considering the $p(d)=0.5$ and $p(p\nu/d)_U$ equal to 0.7 (due to higher accuracy of this method in comparison with radiography in this sample). Figs. 11(c), (d), and (e) were obtained by using the $p(p\nu/d)_R$ value equal to 0.2, 0.5, and 0.7, respectively. These findings disclosed that increasing the conditional probability value of the radiography method led to the increase in the knowledge of this method. It was noticeable that the integration method had the most compatibility with the ideal image (Fig. 8(a)). These results were in accordance with those of Gros et al. [30].

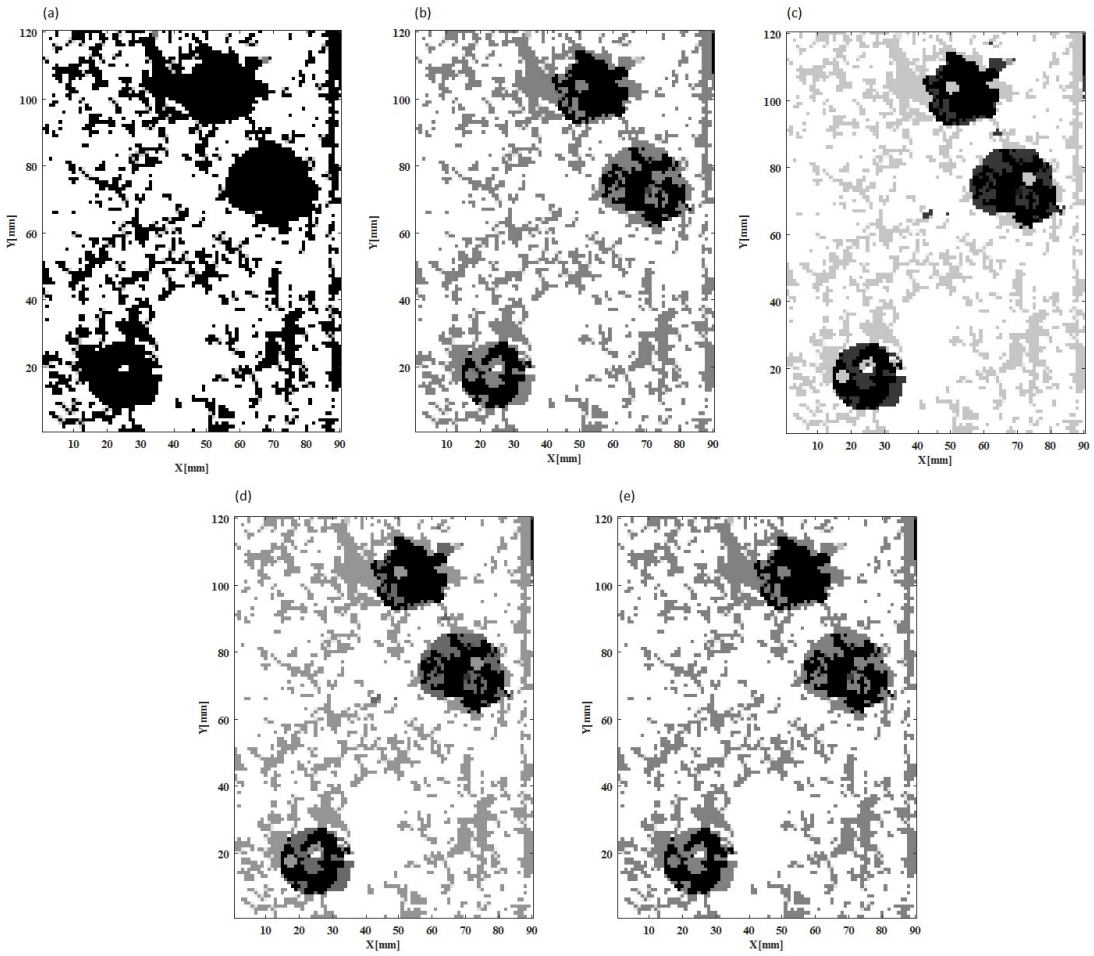

Fig. 11. The result of data fusion from NDT images resulting from (a) integration method, (b) maximum amplitude method and Bayesian analysis with $p(d)=0.5$ and $p(p\nu/d)_U = 0.5$ and (c) $p(p\nu/d)_R = 0.2$, (d) $p(p\nu/d)_R = 0.5$ and (e) $p(p\nu/d)_R = 0.5$.

Fig. 12(a) shows the superposition of binary X-ray radiography and ideal images. In this figure, defects in the binary X-ray radiographic image are shown in black and defects in the ideal image are indicated in green. There are many areas in X-ray radiography results that are wrongly identified as defect areas. Fig. 12(b) demonstrates the superposition of binary C-scan and ideal images. In this figure, defects in the binary C-scan image are displayed in white and defects in the ideal image are shown in green. As can be seen, there is an appropriate match between these two images. On the other hand, the use of the ultrasonic C-scan method is more time-consuming and costly and requires more skill to process the signals. However, it has a higher

accuracy and gives better results for the GFPR specimen. In comparison, the X-ray radiography is a very simple method. Accordingly, the choice of the best NDT method depends on the type of the material.

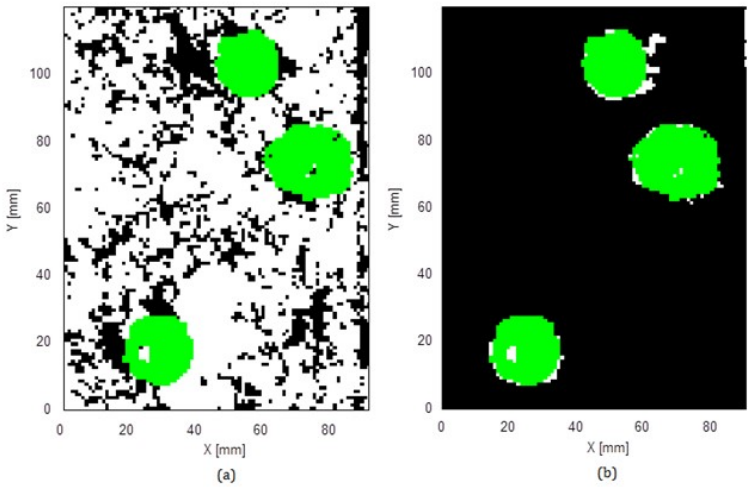

Fig. 12. (a) Superimposed binary image of X-ray result (black) on the binary digital scan (green) of the specimen and (b) Superimposed binary image of the ultrasonic C-scan result (green) on the binary digital scan (white) of the specimen.

4. Conclusions

Today, composite materials are widely used in industries and structures because of their favorable properties. However, the defect and impact damage may develop during the production or service time of these materials. Therefore, NDT methods play a key role in the material quality inspection. The accuracy of various NDT methods depends on the type and the application of materials. This study introduced MSE and PSNR formulas as procedures to compare NDT methods for the impact damage detection in the GFRP specimen. It was found that the MSE value was higher for the X-ray radiography while the PSNR was larger for the ultrasonic C-scan method. The results revealed that ultrasonic C-scan is a better method for impact detection in the GFRP materials. This procedure opens up the scope for future work in this area to assess the accuracy of other NDT methods for various materials.

Conflict of Interest

The authors declare no conflict of interest.

References

[1] Hutchins, D.A., Pardoe, A.C., Billson, D.R., Hines, D.L., Neural network correction of ultrasonic C-scan images, *Ultrasonic*, 37(4), 1999, 263-272.

[2] He,Y., Tian, G. Y., Pan, M., Chen, D., Non-destructive testing of low-energy impact in CFRP laminates and interior defects in honeycomb sandwich using scanning pulsed eddy current, *Composites: Part B*, 59(1), 2014,196-203.

[3] Gros, X. E., Takahashi, K., Non-destructive evaluation of the effect of ply orientation on the impact resistance of thermoplastic toughened thermoset resin polymeric matrix composite, *International Conference on Advanced Materials*, Hurghada, Egypt, 8-14, December 15–18, 1998.

[4] Maierhofer, Ch., Myrach, Ph., Reischel, M., Steinfurth, H., Röllig, M., Kunert, M.,Characterizing damage in CFRP structures using flash thermography in reflection and transmission configurations, *Composites: Part B*, 57(1), 2014, 35-46.

[5] Usamentiaga, R., Venegas, P., Guerediaga, J., Vega, L., López, I., Automatic detection of impact damage in carbon fiber composites using active thermography, *Infrared Physics & Technology*, 58(1), 2013, 36-46.

[6] Meola, C., Carlomagno, G. M., Infrared thermography to evaluate impact damage in glass/epoxy with manufacturing defects, *Impact Engineering*, 67(1), 2014, 1-11.

[7] Liang,T., Ren,W., Tian, G.Y., Elradi, M., Gao, Y., Low energy impact damage detection in CFRP using eddy current pulsed Thermography, *Composite Structure*, 143(1), 2016, 352-361.

[8] Cheng, L., Gao, B. Tian, G. Y. Woo, W. L. Berthiau, G. Impact damage detection and identification using eddy current pulsed thermography through integration of PCA and ICA, *IEEE Sensors Journal*, 14(5), 2014, 1655-1663.

[9] Koyama, K., Hoshikawa, H., Hirano, T., Investigation of impact damage of carbon fiber rainforced plastic (CFRP) by eddy current non-destructive testing, *International Workshop Smart Materials, Structures & NDT in Aerospace,* Montreal, Canada, November 2-4, 2011.

[10] Rauter, N., Lammering, R., Impact damage detection in composite structures considering nonlinear lamb wave propagation, *Mechanics of Advanced Materials and Structures*, 22(1-2), 2014, 44-51.

[11] Capriotti, M., Kim, H.E., Scalea, F.L.D., Kim, H., Non-Destructive inspection of impact damage in composite aircraft panels by ultrasonic guided waves and statistical processing, *Materials*, 10(6), 2017, 1-12.

[12] Hasiotis, Th., Badogiannis, E., Tsouvalis, N. G., Application of ultrasonic c-scan techniques for tracing defects in

laminated composite materials, *Journal of Mechanical Engineering*, 57(3), 2011, 192-203.
[13] Shen, Q., Omar, M., Dongri, Sh., Ultrasonic NDE techniques for impact damage inspection on CFRP laminates, *Journal of Materials Science Research*, 1(1), 2012, 2-16.
[14] Ono, K., Mizutani, Y., Takemoto, M., Analysis of acoustic emission from impact and fracture of CFRP laminates, *Journal of Acoustic Emission*, 25(1), 2007, 179-186.
[15] Amoroso, M.P., Caneva, C., Nanni, F., Valente, M., Acoustic emmision performance for damage monitoring of impacted FRP Composites Laminates, *Review of Quantitative Nondestructive Evaluation*, 22(1), 2003,1447- 1454.
[16] Chandarana, N., Sanchez, D. M., Soutis, C., Gresil, M., Early damage detection in composites during fabrication and mechanical testing, *Materials*, 10 (7), 2017, 1-16.
[17] Yunze, H., Ruizhen, Y., Hong, Zh., Deqiang, Zh., Gang, W., Volume or inside heating thermography using electromagnetic excitation for advanced composite materials, *International Journal of Thermal Sciences*, 111, 2017, 41-49.
[18] Yunze, H., Sheng, Ch., Deqiang, Zh., Shoudao, H., Pan, W., Shared Excitation Based Nonlinear Ultrasound and Vibro-Thermography Testing for CFRP Barely Visible Impact Damage Inspection*, IEEE Transactions on Industrial Informatics*, 2018, 1-10.
[19] Cantwell, W.J., Morton, J., Detection of impact damage in CFRP laminates, *Composite Structures*, 3(3), 1985, 241-257.
[20] Ravikiran, N. K., Venkataramanaiah, A., Bhat, M.R., Murthy, C.R.L., Detection and evaluation of impact damage in CFRP laminates using ultrasound c-scan and IR thermography, *National Seminar on Non- Destructive Evaluation*, Hyderabad, India, 1-5, December 7-9, 2006.
[21] Chambers, A.R., Heinje, N.O., Damage charactrisation in CFRP using acoustic emission, X-Ray tomography and FBG Sensors, *17 th international conference on composite material*, Edinburgh, England, 12-22, July 27-31, 2009.
[22] Pieczonka, L., Aymerich, F., Staszewski, W. J., Impact damage detection in light composite sandwich panels, *Procedia Engineering*, 88(1), 2014, 216 – 221.
[23] Nasirzadeh, R., Sabet, A. R., Influence of nanoclay reinforced polyurethane foam toward composite sandwich structure behavior under high velocity impact, *Journal of Cellular Plastics*, 52(3), 2015, 253-275.
[24] Summerscales, J., *Non-destructive testing of fibre-reinforced plastics composites*, London, Elsevier applied science, 1987, 1-24.
[25] Thung, K. H., Raveendran, P., *A survey of image quality measures*, Proc. International Conference for Technical Postgraduates (TECHPOS), Kuala Lumpur, Malaysia, 1-4, December 14-15, 2009.
[26] Mohammadi, P., Ebrahimi-Moghadam, A., Shirani, SH., Subjective and Objective Quality Assessment of Image: A Survey, *Majlesi Journal of Electrical Engineering,* 9(1), 2015, 55-83.
[27] Sasi varnan, C., Jagan, A., Kaur, J., Jyoti, D., Rao, D.S., Gait Recognition Using Extracted Feature Vectors, *International Journal of Computer Science and Technology*, 2(3), 2011, 2229-4333.
[28] Dhull, S., Arya, S., Sahu, O.P., Applications Comparison of Time-Delay Estimation Techniques in Acoustic Environment, *International Journal of Computer Application*s, 8(9), 2010, 29-31.
[29] Tamim, N.Sh.M., Ghani, F., Techniques for Optimization in Time Delay Estimation from Cross Correlation Function, *International Journal of Engineering & Technology*, 10(2), 2010, 49-54.
[30] Gros, X. E., Bousigue, J., Takahashi, K., NDT data fusion at pixel level, *NDT&E International*, 32, 283–292, 1999.
[31] Heideklang], R., Shokouhi, P., Application of Data Fusion in Nondestructive Testing (NDT), *Proceedings of the 16th International Conference on Information Fusion,* Istanbul, Turkey, 9-12 July 2013.
[32] Mihai, A., Stefanescu, F., mitrache, A. D., Neagu, G., *Composite Materials Flaws etection and Measurement by Infrared Thermography*, 12th Quantitative Infrared Thermography Conference, Bordeaux, France, 1-6, July 7-11, 2014.
[33] Rashli, R., Abu Bakar, E., Othman, A.R., *Feature analysis of ultrasonic C-scan image for non-destructive evaluation*, Proceedings of the IIEEJ image electronics and Visual Computing Workshop, Kuching, Malaysia, November 21-24, 2012.
[34] J. He, Q. D. M. Do, A. C. Downton and J. H. Kim, *A Comparison of Binarization Methods for Historical Archive Documents*, ICDAR '05 Proceedings of the Eighth International Conference on Document Analysis and Recognition, Seoul, Korea, 538-542, August 31-September 1, 2005.